Monthly Notices of the ROYAL ASTRONOMICAL SOCIETY

MNRAS **522,** 1662–1668 (2023)
Advance Access publication 2023 April 6

https://doi.org/10.1093/mnras/stad1027

uGMRT observations of the hot-Saturn WASP-69b: Radio-Loud Exoplanet–Exomoon Survey II (RLEES II)

Mayank Narang [1,2★] Apurva V. Oza [3] Kaustubh Hakim [4,5] P. Manoj,[2] Himanshu Tyagi,[2] Bihan Banerjee,[2] Arun Surya,[2] Prasanta K. Nayak [2] Ravinder K. Banyal[6] and Daniel P. Thorngren[7]

[1]*Academia Sinica Institute of Astronomy & Astrophysics, 11F of Astro-Math Bldg., No. 1, Sec. 4, Roosevelt Road, Taipei 10617, Taiwan, R.O.C.*
[2]*Tata Institute of Fundamental Research (TIFR), Mumbai, Maharashtra 400005, India*
[3]*Jet Propulsion Laboratory (JPL), Caltech 4800 Oak Grove Dr, Pasadena, CA 91109, USA*
[4]*KU Leuven, Institute of Astronomy, Celestijnenlaan 200D, B-3001 Leuven, Belgium*
[5]*Royal Observatory of Belgium, Ringlaan 3, B-1180 Brussels, Belgium*
[6]*Indian Institute of Astrophysics (IIA), 2nd Block, 100 Feet Rd, Koramangala, Bangalore, Karnataka 560034, India*
[7]*Department of Physics and Astronomy at Johns Hopkins University Baltimore, MD 21210, USA*

Accepted 2023 March 30. Received 2023 March 30; in original form 2023 February 8

ABSTRACT

Exomoons have so far eluded ongoing searches. Several studies have exploited transit and transit timing variations and high-resolution spectroscopy to identify potential exomoon candidates. One method of detecting and confirming these exomoons is to search for signals of planet-moon interactions. In this work, we present the first radio observations of the exomoon candidate system WASP-69b. Based on the detection of alkali metals in the transmission spectra of WASP-69b, it was deduced that the system might be hosting an exomoon. WASP-69b is also one of the exoplanet systems that will be observed as part of *JWST* cycle-1 GTO. This makes the system an excellent target to observe and follow up. We observed the system for 32 h at 150 and 218 MHz using the upgraded Giant Metrewave Radio Telescope (uGMRT). Though we do not detect radio emission from the systems, we place strong 3σ upper limits of 3.3 mJy at 150 MHz and 0.9 mJy at 218 MHz. We then use these upper limits to estimate the maximum mass-loss from the exomoon candidate.

Key words: planets and satellites: aurorae – planets and satellites: gaseous planets – planets and satellites: magnetic fields – planet–star interactions – radio continuum: planetary systems.

1 INTRODUCTION

The discovery of an exomoon is the next natural step in the galactic hierarchy of celestial objects. Signatures of alkali metals such as Na and K have been reported in the high-resolution spectra of about 20 transiting giant exoplanets (e.g. Charbonneau et al. 2002; Wyttenbach et al. 2017). By analogy with the Na escape signature from the Jupiter-Io system, Oza et al. (2019) proposed that ionizing alkali clouds fueled by evaporative mass-loss from exomoons orbiting these exoplanets can explain the observed alkaline exospheres of transiting exoplanet systems (Wyttenbach et al. 2017; Gebek & Oza 2020).

The finding by Cassidy et al. (2009) that exomoons around close-in gas giant exoplanets have stable orbits over astronomical time-scales led to the demonstration that the stellar tide will melt the interiors of exomoons and evaporate their surfaces. In our Solar system, due to tidal heating, Io exhibits evaporation in the form of extreme mass-loss $\sim$1000 kg s^{-1}. While Io's eccentricity and tidal heating are due to Europa and Ganymede locking it into a Laplace resonance (4:2:1) around Jupiter's gravitational well (Peale, Cassen & Reynolds 1979), exomoons of close-in exoplanets have a large periodic eccentricity due to stellar forcing (Cassidy et al. 2009). The impact of the stellar tide on the tidal heating rate ($\dot{E}_s$) is a strong inverse function of the planet's orbital period (τ_p): $\dot{E}_s \propto \tau_p^{-5}$ (Cassidy et al. 2009). The evaporation limit for an Io-mass exomoon orbiting a gas giant was found (Oza et al. 2019) to be within a critical orbital period of $\tau_c = 1$ d (for hydrodynamic mass-loss, Perez-Becker & Chiang 2013) and $\tau_c = 2.6$ d (for tidally driven mass-loss, Charnoz et al. 2021; but see Dobos et al. 2021) consistent with the dearth of evaporated metals within the radius resulting from this critical period.

Transiting exoplanets are ideal candidates for exo-Ios because they allow for transit follow-ups with *JWST*. However, an independent detection of these exomoons is necessary before considerable telescope time is devoted to investigating them. One method of detecting exomoons is by observing the radio emissions due to exoplanet–exomoon interaction.

The Io-controlled decametric (Io-DAM) emission (Bigg 1964) is one such example of planet-moon interaction that leads to a detectable signal. These emissions are generated by the interaction between Io and Jupiter's magnetic field. Io is a highly volcanic moon, and the volcanoes on its surface emit a large amount of ionized gas. Due to ongoing volcanism, the moon possesses an atmosphere of highly ionized SO_2 (Lellouch, McGrath & Jessup 2007), which produces an ionosphere around the moon. This ionized gas is then captured by Jupiter's strong magnetic field, forming a plasma torus around the planet (see Fig. 1). As Io orbits within this plasma torus,

★ E-mail: mnarang@asiaa.sinica.edu.tw

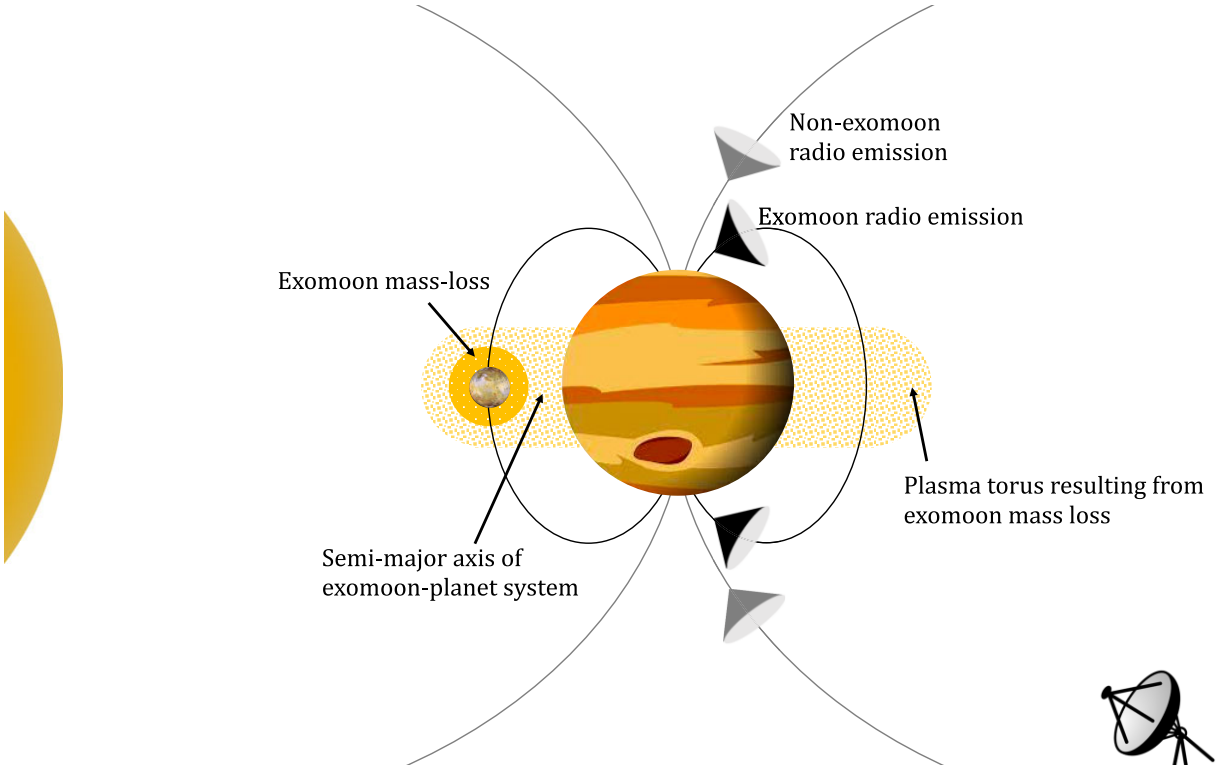

Figure 1. A schematic representation of the ECMI emission process between an exoplanet, exomoon, and exoplasma-torus. The satellite semimajor axis a_s is defined by dynamics and stability criteria (Cassidy et al. 2009), the mass-loss by stellar tides and irradiation (Oza et al. 2019), and the scale height defines the volume of the plasma torus responsible for the beamed emission S_{ν_c}. The cyclotron frequency $\nu_c = 2.8\ B_p$ determines the selected observational frequency and can result in non-exomoon emission (gray cone) and radio-loud exomoon-exoplanet emission (black cone) based on the field strength at the satellite orbit $B_s \sim B_p\ (R_p/a_s)^3$.

it generates a current that flows between the moon and the planet (Goldreich & Lynden-Bell 1969; Grießmeier, Zarka & Spreeuw 2007), giving rise to an unipolar inductor. The interaction between Io and the plasma torus also generates magnetic field oscillations known as Alfvén waves (Belcher 1987), which leads to the production of electric fields parallel to the Jovian magnetic field line (Neubauer 1980; Crary 1997; Saur 2004). The electrons then accelerate along magnetic field lines, whose gyration produces radio emission via an electron cyclotron maser instability (ECMI) process (e.g. Wu & Lee 1979; Treumann 2006). If a similar mechanism also operates in exomoon–exoplanet systems, then their emission might also be detectable, making these exomoons 'Radio-loud', similar to Io.

Several attempts have been made to detect radio emissions from exoplanets, but no successful detection has yet been reported (see Griessmeier 2017; Lazio 2018; Narang et al. 2021a, b; Turner et al. 2021). However, radio emission due to star-planet interaction from the star has been reported in a few cases (e.g. Vedantham et al. 2020; Callingham et al. 2021). Recently Narang et al. (2023) carried out the first dedicated search to detect radio emissions from a sample of exoplanets that showed possible signatures of an exomoon in their transmission spectra. Though no detections were made in that survey, it opened up the possibility of using radio observations to search for exomoons. Discovery of exomoons via radio emission hinges on several factors, including observing the emission at the correct frequency (which in turn depends on the magnetic field of the exoplanets, which are largely unknown), the emission being beamed towards us during our observation run, the evaporation from the exomoon being powerful enough to lead to a detectable signature. All these make the detection of radio emissions from planet-moon interactions a challenging but plausible experiment.

In this work, we present our observation of the hot-Saturn WASP-69b using the upgraded Giant Metrewave Radio Telescope (uGMRT) to study the planet-moon interaction and search for a volcanic exomoon. The star WASP-69 is a K5 star at a distance of 50 pc (Bailer-Jones et al. 2021). The WASP-69 system is host to WASP-69b, a hot-Saturn with a mass of $0.26 \pm 0.017\ M_J$ (radius of $1.057 \pm 0.047\ R_J$) and an orbital period of 3.86 d (0.045 au, Anderson et al. 2014). A strong signature of Na was reported by Casasayas-Barris et al. (2017). The atmosphere of WASP-69b has been studied widely with ground-based high-resolution spectroscopy and *Hubble Space Telescope* (Nortmann et al. 2018; Estrela et al. 2021). Oza et al. (2019) attributed the Na detection in the atmosphere of WASP-69b to the presence of an exo-Io.

Furthermore, the system WASP-69b will be observed as a cycle-1 *JWST* GTO target with both Near Infrared Camera (NIRCam) (proposal ID 1185 Greene et al. 2017b) and Mid-Infrared Instrument (MIRI) (proposal ID 1177 Greene et al. 2017a). These data sets may possess infrared signatures of hot spots of a tidally heated exomoon (Peters & Turner 2013), which may be evident in NIRCAM and MIRI observations. This makes WASP-69b not just an excellent candidate for uGMRT observations but also for follow-up ground and space-based observations. WASP-69b was previously observed at 150 MHz with GMRT as part of the TIFR GMRT Sky Survey (TGSS; Intema et al. 2017). The TGSS observations reached an rms of 2.2 mJy (see Fig. 2). However, no emission was detected from the source.

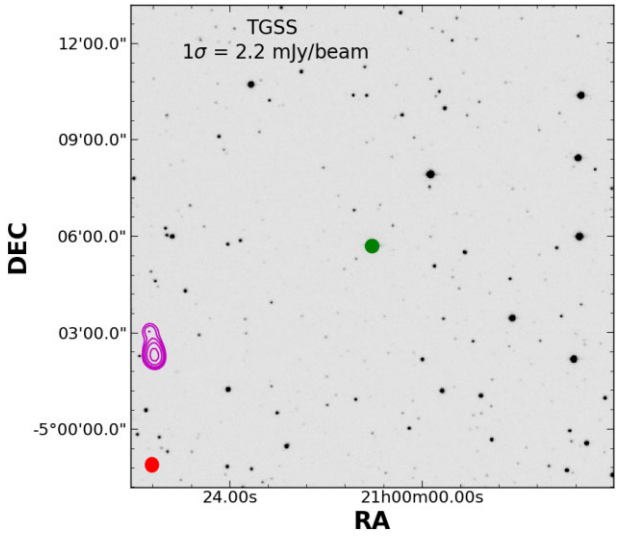

Figure 2. The TGSS 150 MHz GMRT image (magenta contours) of the WASP-69 field at 150 MHz overlaid on the ztf *g*-band image. The green circle marks the position of the WASP-69. The contours plotted are 5, 7, 10, 15, and 25 $\times\,\sigma$. The beam is shown as a red ellipse at the bottom left corner.

Table 1. Summary of observation and the rms sensitivity reached during our observation run.

Date of observation –	Start time – (UTC)	Duration – (h)	rms 150 MHz (mJy/b)	rms 218 MHz (mJy/b)
2021 Nov 05^{th}	0830	7	5.5	0.5
2021 Nov 06^{th}	1030	7	1.1	0.4
2021 Nov 07^{th}	0830	6	4.9	0.3
2021 Nov 08^{th}	0830	6	4.3	0.3
2021 Nov 09^{th}	0830	6	2.2	0.5

In Section 2, we describe the details of the observations and the data reduction process. Next, we present our findings and discuss them in Section 3, followed by a summary in Section 4.

2 OBSERVATION AND DATA REDUCTION

The WASP-69 system was observed for 32 h with uGMRT (proposal ID 41_068, PI Kaustubh Hakim). We observed the system in the band-2 (120–250 MHz) of uGMRT. The system was observed for 5 consecutive days. At each pointing, the system was observed for 6–7 h. The complete log of the observations is listed in Table 1. For all five pointings, the observation setup was the same. The flux calibrator 3C286 was observed at the beginning of the observation, while the flux calibrator 3C48 was observed at the end of the observation run. We observed the phase calibrator 2047–026 in a loop with the target WASP-69 with 27 min of WASP-69 and 6 min on the phase calibrator 2047–026.

To reduce the band-2 (120–250 MHz) uGMRT data, we used Source Peeling and Atmospheric Modeling (SPAM) pipeline (Intema et al. 2009; Intema 2014a, b). SPAM is a python-based extension to Astronomical Image Processing System (Greisen 2003). SPAM was developed to reduce low-frequency radio interferometric observations using telescopes such as GMRT. SPAM has inbuilt routines for flagging radio frequency interference (RFI) and bad data. SPAM also includes direction-dependent ionospheric calibration and image-plane ripple suppression, which can further improve the image quality. However, the SPAM pipeline does not support the processing of large fractional bandwidths ($\delta f/f > 0.2$). Thus natively, the SPAM is not capable of reducing the wideband data from uGMRT. A workaround for this is to split the bandwidth into smaller chunks (sub-bands) that can be processed independently. The calibrated output visibilities can then be jointly imaged to produce the final image.

The band-2 (120–250 MHz) of uGMRT has a break in the middle (165–185 MHz) and can be divided into two frequency ranges. Thus we decided to split band-2 into two different subbands with a bandwidth of about ∼30 MHz around regions of relatively low radio frequency interference. We selected channel numbers from 600–1100 (500 channels) corresponding to a band center of ∼218 MHz and channel numbers from 1350–1750 (400 channels) corresponding to a band center of ∼150 MHz. These channels were relatively free of RFI. Therefore, we processed the two sub-bands independently and produced the final images. The rms noise of these two sub-bands is very different, so we decided not to combine the two images to produce a wideband image.

3 RESULTS

3.1 Observed upper limits on the radio flux density

The WASP-69 system was observed with uGMRT for 5 d in band-2 (120–250 MHz), totaling 32 h. In Fig. 3, we show the band-2 150 MHz images of the WASP-69 field, while in Fig. 4, we show the band-2 218 MHz images of the WASP-69 field. In Table 1, we have listed the rms reached during these observations. The rms value for the WASP-69 field ranges from 1.1–5.5 mJy beam^{-1} at 150 MHz and between 0.3–0.5 mJy beam^{-1} at 218 MHz. Using the lowest value of rms and assuming 3× *rms* as an upper limit to the radio flux density S_ν, we get $S_\nu = 3.3$ mJy at 150 MHz and $S_\nu = 0.9$ mJy at 218 MHz. Our observations at 218 MHz are some of the deepest observations that have been carried out at these frequencies (e.g. Lecavelier Des Etangs et al. 2009, 2011; O'Gorman et al. 2018; Narang et al. 2021b; Narang 2022).

3.2 Maximum radio power

The maximum radio power P_ν emitted by the exoplanet–exomoon system can be calculated from the observed upper limits on the radio flux density (e.g. Lazio et al. 2004; Grießmeier et al. 2007): $P_\nu = S_\nu \Delta\nu\, \Omega d^2$, where $\Delta\nu$ is the bandwidth of emission such that $\Delta\nu = \nu_c/2$, $\Omega = 0.16$ (average value of Io-DAM Zarka, Cecconi & Kurth 2004) is the angle of the emission cone, and d is the distance of the exoplanet from Earth. We find the maximum radio power that could be emitted from the WASP-69 system is 9×10^{14} W (at 150 MHz) and 4×10^{14} W (at 218 MHz). Compared to the maximum radio power emitted from the Io Flux Tube (IFT) of $\sim 10^8$–10^{10} W (Bhardwaj, Randall Gladstone & Zarka 2001), our upper limits are $10^{4.9}$–$10^{6.9}$ times higher at 150 MHz and $10^{4.6}$–$10^{6.6}$ times higher at 218 MHz.

3.3 Constraining the mass-loss rate from the exomoon

The maximum emitted radio power from an exoplanet–exomoon interaction depends on the plasma mass density and the magnetic field (Neubauer 1980). At low plasma densities, the radio power P_- scales linearly with the magnetic field at the satellite location, B_s, and as the square root of plasma mass density ρ_s. At high plasma densities, the radio power P_+ scales with the square of the magnetic

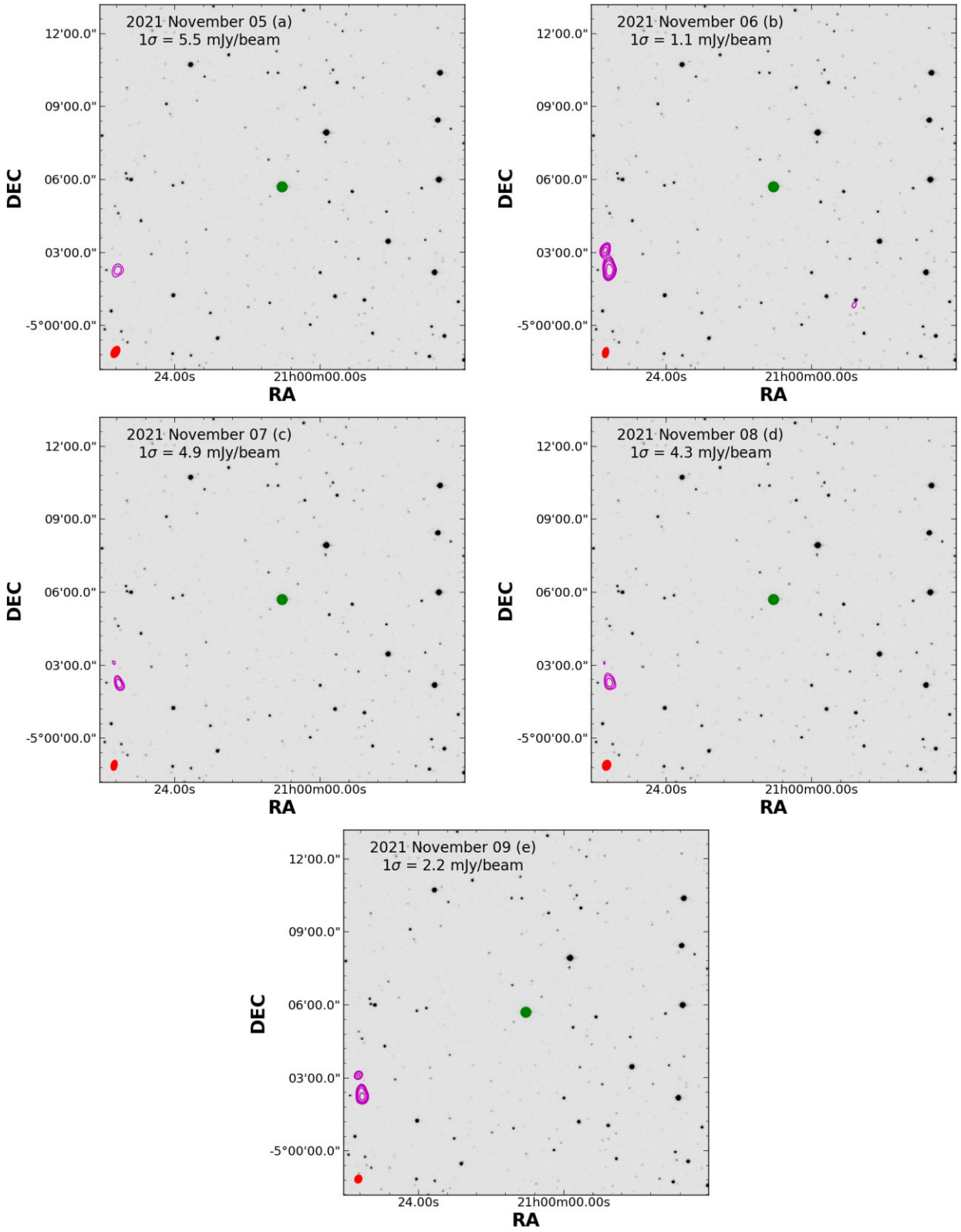

Figure 3. The uGMRT image (magenta contours) of the WASP-69 field at 150 MHz for each individual observation night overlaid on the ztf *g*-band image. The green circle marks the position of the WASP-69. The contours plotted are 5, 7, 10, 15, and 25 $\times\,\sigma$. The beam is shown as a red ellipse at the bottom left corner.

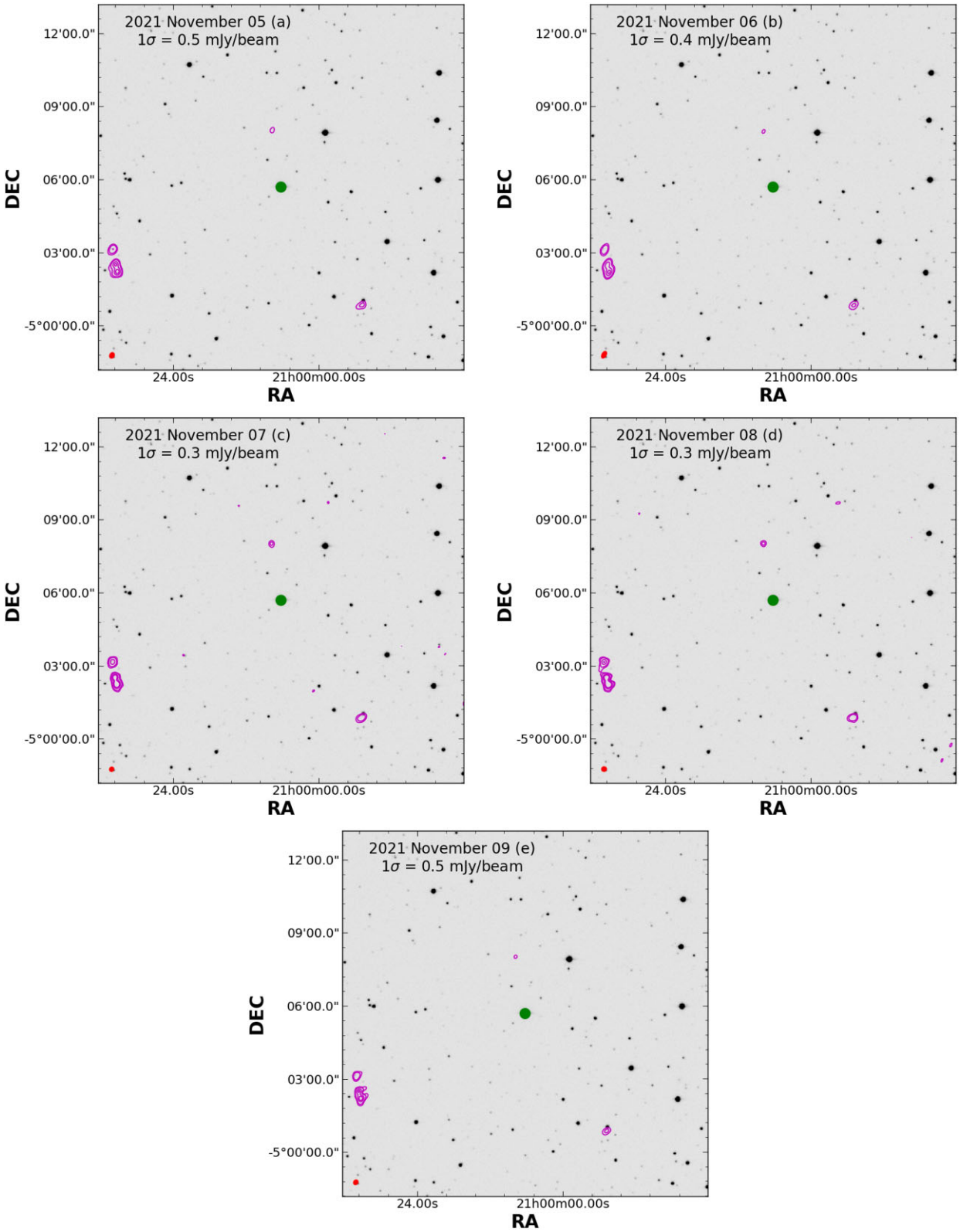

Figure 4. The uGMRT image (magenta contours) of the WASP-69 field at 218 MHz for each individual observation night overlaid on the ztf *g*-band image. The green circle marks the position of the WASP-69. The contours plotted are 5,10, 30, and 50 $\times\,\sigma$. The beam is shown as a red ellipse at the bottom left corner.

field and is independent of plasma mass density (Noyola, Satyal & Musielak 2014),

$$P_{-} \propto B_{\rm s}\sqrt{\rho_{\rm s}}, \tag{1}$$

$$P_{+} \propto B_{\rm s}^2. \tag{2}$$

Although the determination of the magnitude of plasma density is beyond the scope of this paper, these two limits can be used to make qualitative arguments on the mass-loss rate from the exomoon $\dot{M}$, which scales linearly with plasma density: $\dot{M} \propto \rho_{\rm s}$. Moreover, for a given planetary magnetic field B_0, the magnetic field at the satellite location drops as $B_{\rm s} \propto B_0/a_{\rm s}^3$ (see Section 4.1 for discussion on magnetic field strength). Therefore, at the lower limit of plasma density, the mass-loss rate from the exomoon is proportional to the sixth power of the exomoon semimajor axis,

$$\dot{M} \propto \left(\frac{P_{-}}{B_{\rm s}}\right)^2 = \left(\frac{P_{-}}{B_0}\right)^2 a_{\rm s}^6. \tag{3}$$

For stable exomoons, the value of $a_{\rm s}$ is between the Roche limit and half the hill radius (Cassidy et al. 2009). For WASP-69b, this range for a satellite having a composition similar to Io is between 1.16–2.1 $R_{\rm J}$ (Oza et al. 2019). This is much closer than the orbital distance of 5.9 $R_{\rm J}$ of Io around Jupiter. Taking $a_{\rm s} = 1.63\,R_{\rm J}$ (average of the Roche limit and half the Hill radius), the minimum radio power ratio of WASP-69b to IFT of $10^{4.9}$ at 150 MHz, and the magnetic field ratio of $\sim$13 ($B_{0,\rm W69b} = 54$ G at 150 MHz, which is fixed by the search frequency, $\nu = 2.8\,B_0$ and cf. $B_{0,\,\rm Jup} = 4.17$ G), we find that the mass-loss rate from a hidden exo-Io is roughly 17 000 times higher than Io. However, to better constrain the mass-loss from the system, further observations of the companion alkali doublet K predicted to be roughly $\sim$10 $\times$ less abundant than Na (Gebek & Oza 2020), are required in ground-based high-resolution spectroscopy. With NIRCAM/MIRI (proposal ID 1185 and 1177) and *JWST*, volcanically vented molecules such as SO_2 CO_2 and CO are expected to be apparent due to tidally heated volcanism as seen at Io from both ground-based (CRIRES/VLT; Lellouch et al. 2015) and space-based spectrographs (JIRAM/JUNO; Mura et al. 2020).

4 DISCUSSION

There could be several reasons why no radio emission was detected from these systems. In the following subsection, we discuss some of them.

4.1 Cyclotron frequency and gas giant magnetic field strength

The cyclotron frequency $\nu_{\rm c}$ for emission is given as $\nu_{\rm c} = 2.8\,B_0$, where B_0 is in Gauss and $\nu_{\rm c}$ in MHz. The choice of observing the system in band-2 (120–250 MHz) of uGMRT was based on hot-Saturns having magnetic fields of $\sim$40–100 G (Yadav & Thorngren 2017). If the magnetic field is not within this range, we would not detect it. Furthermore, the probable detection of radio emission from the hot Jupiter τ Boötis b by Turner et al. (2021) between 15 and 30 MHz has challenged the notion of hot-Jupiters and hot-Saturns having a strong magnetic field. Turner et al. (2021) estimate the magnetic field of τ Boötis b to be in the range of 5–11 G. If WASP-69b also possesses such a small magnetic field, then no emission would be detectable in the band-2 (120–250 MHz) of uGMRT. To test this hypothesis, we further computed the magnetic field of WASP-69b. We followed the formalism from Yadav & Thorngren (2017) to estimate the magnetic fields. We used the evolution models from Thorngren & Fortney (2018) to derive the heat flux from the interiors of the planets (also see Christensen, Holzwarth & Reiners 2009). The magnetic field on the dynamo surface is given as (from Reiners & Christensen 2010)

$$B_{\rm rms}^{\rm dyn}\,[\rm G] = 4.8 \times 10^3 (M_{\rm P} L_{\rm P}^2)^{1/6} R_{\rm P}^{-7/6}, \tag{4}$$

where $M_{\rm P}$, $L_{\rm P}$, and $R_{\rm P}$ are the mass, luminosity, and radius of the planet (all normalized to solar values). Assuming scaling law for the dynamo radius from Yadav & Thorngren (2017), the dipole magnetic field strength at the pole is thus

$$B_{\rm dipole}^{\rm polar} = \frac{B_{\rm rms}^{\rm dyn}}{\sqrt{2}} \left(\frac{R_{\rm dyn}}{R_{\rm P}}\right)^3, \tag{5}$$

where $R_{\rm dyn}$ is the dynamo radius. By plugging in the values for the WASP-69 system, we estimate the $B_{\rm dipole}^{\rm polar} = 15$ G. This gives $\nu_{\rm c} =$ 42 MHz. This is much lower than the frequency at which we observed the system.

4.2 Time variable emission

The decameter emission from Jupiter due to the interaction between Jupiter and Io or Jupiter and the solar wind is modulated with a period of a few milliseconds to months (Zarka et al. 1996; Lecacheux, Konovalenko & Rucker 2004; Ryabov et al. 2014; Marques et al. 2017). The emission from exo-moons can also be highly time variable and modulated with the moon's phase around the planet. The emission from these exomoons can be highly beamed (e.g. Queinnec & Zarka 1998; Zarka et al. 2004; Lamy et al. 2022) and emitted in a narrow cone. In such a case, the emission will only be observable during certain phases of the moon around the planet and the planet around its host star. During our observation run, we cover about 35 per cent (32 h/92.6 h of the orbital phase of the planet. However, if the emission cone was not pointed towards Earth, we would miss it.

4.3 Exomoon flux density

As stated in Narang et al. (2023), radio emission due to exomoon-exoplanet interaction can be inherently weak. If the mass-loss rate from the exomoon is lower, then we will not be able to detect any emission. Furthermore, WASP-69 is located at 50 pc, and with our current sensitivity of telescopes, we will not be able to detect any signal if the strength of the radio emission from the system is at the same level as IFT. The next generation of telescopes with high sensitivity are perhaps required for the detection of radio emission arising from exoplanet–exomoon interaction.

5 SUMMARY

This work presents the first radio observations of the exoplanetary system WASP-69 using uGMRT. The WASP-69 system is an exo-Io candidate system based on the presence of strong alkali metal lines in the transmission spectra of the planet (Oza et al. 2019). The WASP-69 system was observed in band-2 (120–250 MHz) of uGMRT. For this analysis, we divided band-2 of uGMRT into two sub-bands at 150 and 218 MHz. We observed the WASP-69 field for 32 h covering about 20 per cent of the orbital phase of the planet over five pointings. At 150 MHz, we achieved a 3σ upper limit of 3.3 mJy, while an upper limit of 0.9 mJy was obtained at 218 MHz. However, no radio emission was detected from the system. This implies that the exomoon may not be radio-loud at the synchrotron frequencies searched for due to either a lower mass-loss rate from the exomoon or a lower magnetic field strength of the parent planet. Moreover, the emission

could be highly time variable and beamed. Therefore, deeper and more frequent observations at lower radio frequencies of the systems than what is currently possible are thus required to detect exomoons.

The upcoming generation of radio telescopes, including the next-generation Very Large Array (McKinnon et al. 2019) and Square Kilometre Array (SKA; Dewdney et al. 2009), will surpass the current telescopes in sensitivity. This increased sensitivity creates the possibility of detecting faint signals originating from the interaction between exoplanets and exomoons even at a much lower frequency. The magnetic field strength for WASP-69b is estimated to be 15 G, which is similar to the estimates derived for other exoplanets (e.g. Yadav & Thorngren 2017; Narang et al. 2023). The emission generated from the exoplanet–exomoon interaction from exoplanets with such low magnetic field strengths will fall below 100 MHz in frequency. Consequently, the SKA appears to be a well-suited instrument for detecting these elusive exomoons.

ACKNOWLEDGEMENTS

This work is based on observations made with the Giant Metrewave Radio Telescope, which is operated by the NCRA TIFR and is located at Khodad, Maharashtra, India. KH was supported by the FED-tWIN research program STELLA funded by the Belgian Science Policy Office (BELSPO).

DATA AVAILABILITY

The data presented in this article are available on the GMRT archive at https://naps.ncra.tifr.res.in/goa/, and can be accessed with proposal id 41_068.

REFERENCES

Anderson D. R. et al., 2014, MNRAS, 445, 1114
Bailer-Jones C. A. L., Rybizki J., Fouesneau M., Demleitner M., Andrae R., 2021, AJ, 161, 147
Belcher J. W., 1987, Science, 238, 170
Bhardwaj A., Randall Gladstone G., Zarka P., 2001, Adv. Space Res., 27, 1915
Bigg E. K., 1964, Nature, 203, 1008
Callingham J. R. et al., 2021, Nat. Astron., 5, 1233
Casasayas-Barris N., Palle E., Nowak G., Yan F., Nortmann L., Murgas F., 2017, A&A, 608, A135
Cassidy T. A., Mendez R., Arras P., Johnson R. E., Skrutskie M. F., 2009, ApJ, 704, 1341
Charbonneau D., Brown T. M., Noyes R. W., Gilliland R. L., 2002, ApJ, 568, 377
Charnoz S. et al., 2021, Icar, 364, 114451
Christensen U. R., Holzwarth V., Reiners A., 2009, Nature, 457, 167
Crary F. J., 1997, J. Geophys. Res., 102, 37
Dewdney P. E., Hall P. J., Schilizzi R. T., Lazio T. J. L. W., 2009, Proc. IEEE, 97, 1482
Dobos V., Charnoz S., Pál A., Roque-Bernard A., Szabó G. M., 2021, PASP, 133, 094401
Estrela R., Swain M. R., Roudier G. M., West R., Sedaghati E., Valio A., 2021, AJ, 162, 91
Gebek A., Oza A. V., 2020, MNRAS, 497, 5271
Goldreich P., Lynden-Bell D., 1969, ApJ, 156, 59
Greene T. P., Lagage P.-O., Rieke M. J., Schlawin E., 2017a, MIRI observations of transiting exoplanets, JWST Proposal. Cycle 1, ID. #1177
Greene T. P., Beatty T. G., Rieke M. J., Schlawin E., 2017b, Transit Spectroscopy of Mature Planets, JWST Proposal. Cycle 1, ID. #1185
Greisen E. W., 2003, in Heck A.ed., Astrophysics and Space Science Library, Vol. 285, Information Handling in Astronomy – Historical Vistas. Springer, Berlin, p. 109
Grießmeier J. M., Zarka P., Spreeuw H., 2007, A&A, 475, 359
Griessmeier J.-M., 2017, in Fischer G., Mann G., Panchenko M., Zarka P., eds, Proceedings of the 8th International Workshop, Planetary Radio Emissions VIII. Austrian Academy of Sciences Press, Vienna, p. 285
Intema H. T., 2014a, Astrophysics Source Code Library, record ascl:1408.006
Intema H. T., 2014b, in Chengalur J. N., Gupta Y., eds, Astronomical Society of India Conference Series, Vol. 13, SPAM: A Data Reduction Recipe for High-Resolution,Low-Frequency Radio-Interferometric Observations. Astronomical Society of India, p. 469
Intema H. T., van der Tol S., Cotton W. D., Cohen A. S., van Bemmel I. M., Röttgering H. J. A., 2009, A&A, 501, 1185
Intema H. T., Jagannathan P., Mooley K. P., Frail D. A., 2017, A&A, 598, A78
Lamy L. et al., 2022, J. Geophys. Res. (Space Physics), 127, e30160
Lazio T. J. W., 2018, in Deeg H. J., Belmonte J. A., eds, Radio Observations as an Exoplanet Discovery Method, Handbook of Exoplanets. Springer Living Reference Work, Berlin, p. 9
Lazio J., Farrell W. M., Dietrick J., Greenlees E., Hogan E., Jones C., Hennig L. A., 2004, preprint (arXiv:e-print)
Lecacheux A., Konovalenko A. A., Rucker H. O., 2004, Planet. Space Sci., 52, 1357
Lecavelier Des Etangs A., Sirothia S. K., Gopal-Krishna, Zarka P., 2009, A&A, 500, L51
Lecavelier Des Etangs A., Sirothia S. K., Gopal-Krishna, Zarka P., 2011, A&A, 533, A50
Lellouch E., McGrath M. A., Jessup K. L., 2007, in Lopes R. M. C., Spencer J. R., eds, Io After Galileo: A New View of Jupiter's Volcanic Moon. Springer, Berlin, p. 231
Lellouch E., Ali-Dib M., Jessup K. L., Smette A., Käufl H. U., Marchis F., 2015, Icarus, 253, 99
Marques M. S., Zarka P., Echer E., Ryabov V. B., Alves M. V., Denis L., Coffre A., 2017, A&A, 604, A17
McKinnon M., Beasley A., Murphy E., Selina R., Farnsworth R., Walter A., 2019, BAAS, 51, 81
Mura A. et al., 2020, J. Geophys. Res. (Planets), 125, e06508
Narang M., 2022, MNRAS, 515, 2015
Narang M., Manoj P., Ishwara Chandra C. H., 2021a, Res. Notes. AAS, 5, 158
Narang M. et al., 2021b, MNRAS, 500, 4818
Narang M., Oza A. V., Hakim K., Manoj P., Banyal R. K., Thorngren D. P., 2023, AJ, 165, 1
Neubauer F. M., 1980, J. Geophys. Res., 85, 1171
Nortmann L. et al., 2018, Science, 362, 1388
Noyola J. P., Satyal S., Musielak Z. E., 2014, ApJ, 791, 25
O'Gorman E., Coughlan C. P., Vlemmings W., Varenius E., Sirothia S., Ray T. P., Olofsson H., 2018, A&A, 612, A52
Oza A. V. et al., 2019, ApJ, 885, 168
Peale S. J., Cassen P., Reynolds R. T., 1979, Science, 203, 892
Perez-Becker D., Chiang E., 2013, MNRAS, 433, 2294
Peters M. A., Turner E. L., 2013, ApJ, 769, 98
Queinnec J., Zarka P., 1998, J. Geophys. Res., 103, 26649
Reiners A., Christensen U. R., 2010, A&A, 522, A13
Ryabov V. B., Zarka P., Hess S., Konovalenko A., Litvinenko G., Zakharenko V., Shevchenko V. A., Cecconi B., 2014, A&A, 568, A53
Saur J., 2004, J. Geophys. Res. (Space Physics), 109, A01210
Thorngren D. P., Fortney J. J., 2018, AJ, 155, 214
Treumann R. A., 2006, A&AR, 13, 229
Turner J. D. et al., 2021, A&A, 645, A59
Vedantham H. K. et al., 2020, Nat. Astron., 4, 577
Wu C. S., Lee L. C., 1979, ApJ, 230, 621
Wyttenbach A. et al., 2017, A&A, 602, A36
Yadav R. K., Thorngren D. P., 2017, ApJ, 849, L12
Zarka P., Farges T., Ryabov B. P., Abada-Simon M., Denis L., 1996, Geophys. Res. Lett., 23, 125
Zarka P., Cecconi B., Kurth W. S., 2004, J. Geophys. Res. (Space Physics), 109, A09S15

This paper has been typeset from a TEX/LATEX file prepared by the author.